NanoScience and Technology

B. Bhushan
H. Fuchs (Eds.)

Applied Scanning Probe Methods IV

Industrial Applications

Springer

28 Microfabricated Cantilever Array Sensors for (Bio-)Chemical Detection

Hans Peter Lang · Martin Hegner · Christoph Gerber

List of Abbreviations

AFM	atomic force microscopy
MW	molecular weight
PCA	principal component analysis
PEEK	poly-etheretherketone
PDMS	poly-dimethyl-siloxane
PSD	position sensitive detector
RIE	reactive ion etching
SFM	scanning force microscopy
VCSEL	vertical-cavity surface-emitting laser
μFN	microfluidic network

28.1 Introduction

28.1.1 Sensors

A sensor is a device that detects, or senses, a signal. A sensor is also a transducer, i.e. it transforms one form of energy into another or responds to a physical parameter. Transducers can be electrochemical (pH probe), electromechanical (piezoelectric actuator, quartz, strain gauge), electroacoustic (gramophone pick-up, microphone), photoelectric (photodiode, solar cell), electromagnetic (antenna, photocell, tape or harddisk head for storage applications), magnetic (Hall effect sensor), electrostatic (electrometer), thermoelectric (thermocouple, thermo-resistors), electrical (capacitor, resistor) or mechanical (deflection sensors). Sensors either directly indicate a state or a value (mercury thermometer), or use an indicator that indirectly displays the state or value by an analog or digital converter (display, computer).

(Bio-)chemical sensors convert changes of physical or chemical parameters due to the presence of molecules in the environment into a recordable signal (Fig. 28.1).

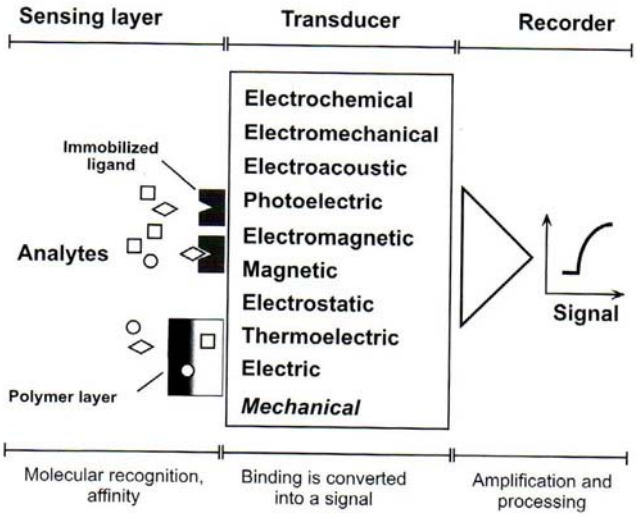

Fig. 28.1. Schematic of general sensor transduction. Analyte molecules present in the environment are recognized by the sensing layer of the sensor. Either recognition is very specific, i.e. recognition sites on immobilized ligand molecules recognize the analyte molecules, or recognition is partially specific, e.g. the analyte molecules diffuse into a polymer layer. The binding event is then transduced into a recordable signal via a variety of transduction mechanisms. The acquired signal is then further amplified and processed

28.1.2 Cantilevers

The term cantilever is understood here as a microfabricated rectangular bar-shaped structure that is longer than it is wide and has a thickness that is much smaller than its length or width. A cantilever is a horizontal structural element supported only at one end on a chip body; the other end is free. At the free end, a microfabricated sharp tip might be attached for use as a local probe to scan a surface. Cantilever beams have been applied since the mid 1980s as sensitive structures to measure interatomic forces in the piconewton range using a technique called scanning force microscopy (SFM) or atomic force microscopy (AFM) [1]. In this method, a cantilever with a sharp tip is scanned across a conductive or nonconductive surface by the use of an x-y-z actuator system (e.g. a piezoelectric scanner). Scanning is performed in a pattern of adjacent parallel lines to cover a rectangular or square area of the sample surface. Typical scanning speeds range from 1 nm/s to several micrometers per second, depending on the size of the area to be scanned. The tip can either be in direct contact with the surface (contact mode) or oscillated to interact with the surface only for a short time during the oscillation cycle (dynamic mode, noncontact mode). Common to SFM methods is the interaction of the cantilever tip with the surface. This interaction can be used to control a feedback loop intended to keep the force or force gradient between cantilever tip and sample surface constant. By recording the correction signal that has to be applied to the z-actuation drive to keep the interaction between tip and sample surface constant, a topography image of the

sample surface can be obtained. SFM methods are nowadays well-established in scientific research, education and to a certain extent also in the industry. Beyond imaging of surfaces, other applications of cantilevers have been demonstrated.

The use of a sharp tip at the cantilever apex is not required for application as the (bio-)chemical sensor described here. Because of their flexibility, cantilevers can not only be used for probing the surface profile of a sample, but also to monitor processes taking place on the surface of the beam [2]. The use of cantilever beams as sensors, clamped at one end and freestanding at the other, allows the adsorption of molecules to be observed with unprecedented accuracy, because the formation of molecule layers on the cantilever surface will generate surface stress. This eventually results in a bending of the cantilever, provided the adsorption preferentially occurs on one surface of the cantilever. Adsorption is controlled by coating one surface (e.g. the upper surface) of a cantilever with a thin layer of a material that shows affinity to molecules in the environment (sensor surface). This surface of the cantilever is referred to as the "functionalized" surface. The other surface of the cantilever (e.g. the lower surface) may be left uncoated or be coated with a passivation layer, i.e. a chemical surface that does not exhibit significant affinity to the molecules in the environment to be detected (see Fig. 28.2). To facilitate the establishment of functionalized surfaces, a metal layer is often evaporated onto the surface designed as sensor surface. Metal surfaces, e.g. a gold surface, may be utilized to covalently bind a monolayer that represents the chemical surface sensitive to the molecules to be detected from environment. A typical example is a monolayer of thiol molecules covalently bound to a gold surface. The gold layer is also favorable for use as a reflection layer, if the bending of the cantilever is read out via an optical beam-deflection method.

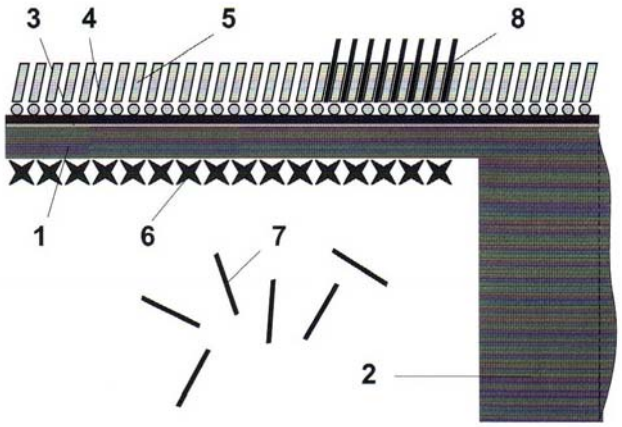

Fig. 28.2. Schematic sideview representation of a functionalized cantilever: (**1**) cantilever beam with a typical thickness of 1 μm, typically made from silicon, (*2*) chip body with a typical thickness of 500 μm, (**3**) 2 nm thick evaporated titanium layer required for adherence of (**4**) a 20 nm thick evaporated gold layer, (**5**) functional sensing layer, e.g. 1 nm thick self-assembled thiol monolayer, (**6**) passivation layer (several nanometers thick), e.g. a silanized polyethyleneglycol layer, (**7**) target molecules from the environment, (**8**) area in which target molecules have docked to the functionalized surface

28.1.3 Cantilever Operating Modes

28.1.3.1 Static Mode

The continuous bending of a cantilever as a function of molecular coverage with molecules is referred to as an operation in the "static mode", see Fig. 28.3. Adsorption of molecules onto the functional layer generates stress at the interface between the functional layer and the forming molecular layer. The stress is transduced towards the site at which the molecules of the functional layer are attached to the cantilever surface. Because the forces within the functional layer try to keep the distance between molecules constant, the cantilever beam responds with bending due to its extreme flexibility. The resulting surface stress change is calculated according to Stoney's formula [3]:

$$\Delta\sigma = Et^2/[4R(1-\nu)]\,, \tag{28.1}$$

where E is Young's modulus ($E_{\mathrm{Si}} = 1.3 \times 10^{11}\,\mathrm{N/m^2}$ for Si(100)), t the thickness of the cantilever, ν Poisson's ratio ($\nu_{\mathrm{Si}} = 0.25$), and R the bending radius of the cantilever.

The static-mode operation can be performed in various environments. In its simplest embodiment, molecules from gaseous environment adsorb on the functionalized sensing surface and form a molecular layer (Fig. 28.3a), provided

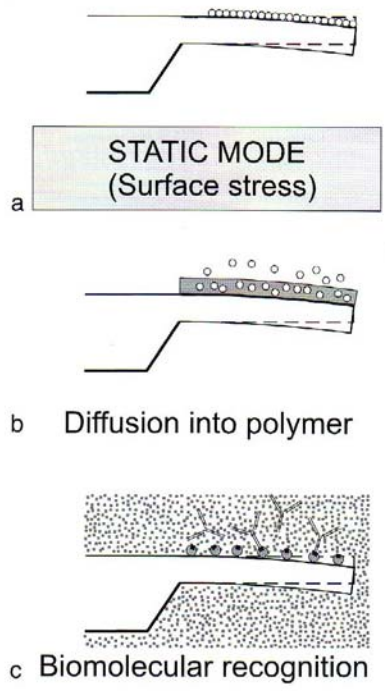

Fig. 28.3. (**a**) Static-mode operation. An adsorbing layer of molecules produces a change in surface stress on the upper functionalized surface of the cantilever, resulting in bending of the cantilever. (**b**) Diffusion of target molecules from the environment into a polymer layer induces swelling of the polymer layer and thereby a bending of the cantilever, because the swollen polymer layer expands more than the silicon cantilever. (**c**) Static-mode operation in liquids. Target molecules from the liquid environment are molecularly recognized by binding sites on the functionalized sensing layer on the upper surface of the cantilever

that the molecules exhibit some affinity to the surface. Polymer sensing layers show a partial sensitivity, because molecules from the environment diffuse into the polymer layer at different rates, mainly depending on the size and solubility of the molecules in the polymer layer (Fig. 28.3b). A wide range of hydrophilic/hydrophobic polymers can be selected, differing in their suitability for polar/unpolar molecules. Thus, the polymers can be chosen according to what the applications demand.

Static-mode operation in liquids, however, usually requires rather specific sensing layers, based on molecular recognition, such as DNA hybridization or antigen-antibody recognition (Fig. 28.3c).

28.1.3.2 Dynamic Mode

Because the bending of the cantilever is a direct result of the adsorbtion of molecules onto the cantilever surface, it is rather difficult to obtain reliable information on the amount of molecules adsorbed, as the surface coverage is basically not known. In addition, molecules on the surface might be exchanged with molecules from the environment in a dynamic equilibrium.

However, mass changes can be determined accurately by operation of a cantilever actuated at its eigenfrequency. The eigenfrequency is equal to the resonance frequency of an oscillating cantilever if the elastic properties of the cantilever remain unchanged during the molecule adsorption process and damping effects are negligible. This operation mode is called the dynamic mode (e.g., the use as a microbalance, Fig. 28.4a). Owing to mass addition on the cantilever surface, the cantilever's eigenfrequency will shift to a lower value. The mass change on a rectangular cantilever is calculated [4] according to

$$\Delta m = (k/4\pi^2) \times \left(1/f_1^2 - 1/f_0^2\right) , \tag{28.2}$$

where f_0 is the eigenfrequency before the mass change occurs, and f_1 the eigenfrequency after the mass change. The spring constant k of the cantilever is obtained using

$$k = Et^3 w/4l^3 , \tag{28.3}$$

where l, w, and t denote the length, width, and thickness of the cantilever, respectively.

Mass-change determination can be combined with varying environment temperature conditions (Fig. 28.4b) to obtain the method introduced in the literature as "micromechanical thermogravimetry" [5]. The sample to be investigated has to be mounted at the apex of the cantilever. Its mass should not exceed several hundred nanograms. In the case of adsorption/desorption/decomposition processes, mass changes in the picogram range can be observed in real time by tracking the resonance-frequency shift.

Dynamic mode operation in liquid environment poses problems, such as high damping of the cantilever oscillation due to high viscosity of the surrounding media.

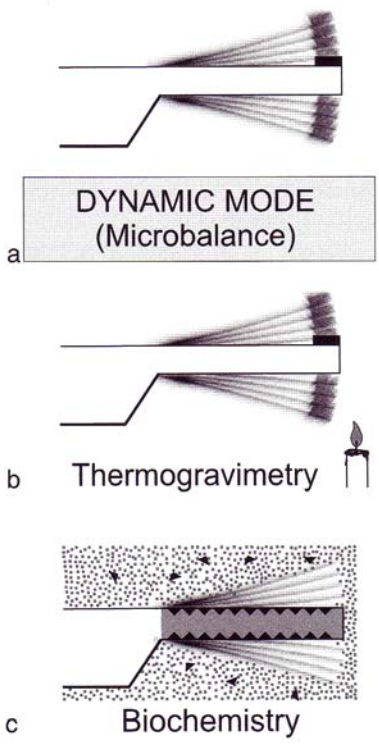

Fig. 28.4. (**a**) Cantilever operation in dynamic mode. The cantilever is excited at its resonance frequency. Tracking the resonance frequency allows one to determine mass changes. (**b**) Micromechanical thermogravimetry. Mass changes are measured in dependence of temperature as an external parameter. (**c**) Detection of biochemical processes involving mass changes due to adsorption and binding of molecules

This results in a low quality factor Q of the oscillation, and the resonance frequency shift is difficult to track with high resolution. The quality factor is defined as

$$Q = 2\Delta f / f_0 \,. \tag{28.4}$$

Whereas in air a frequency resolution of below 1 Hz is easily achieved, resolution values of about 20 Hz are already considered very good for measurements in a liquid environment.

28.1.3.2.1 Operation in a Large Damping Environment

In the case of damping or changes of the elastic properties of the cantilever during the experiment, e.g. a stiffening or softening of the spring constant by adsorption of a molecule layer, the measured resonance frequency will not be exactly the same as the eigenfrequency, and the mass derived from the frequency shift will be inaccurate. In a medium, the vibration of a cantilever is described by the model of a driven damped harmonic oscillator:

$$m^* \frac{\mathrm{d}^2 x}{\mathrm{d}t^2} + \gamma \frac{\mathrm{d}x}{\mathrm{d}t} + kx = F\cos(2\pi f t) \,, \tag{28.5}$$

where $m^* = \text{const.}(m_c + m_l)$ is the effective mass of the cantilever (for a rectangular cantilever the constant is 0.25). Especially in liquids, the mass of the co-moved liquid m_l adds significantly to the mass of the cantilever m_c. The term $\gamma \frac{dx}{dt}$ is the drag force due to damping, $F\cos(2\pi ft)$ is the driving force executed by the piezo-oscillator, and k is the spring constant of the cantilever.

If no damping is present, the eigenfrequencies of the various oscillation modes of a bar-shaped cantilever are calculated according to:

$$f_n = \frac{\alpha_n^2}{2\pi}\sqrt{\frac{k}{3(m_c + m_l)}}\,, \tag{28.6}$$

where f_n are the eigenfrequencies in the n-th mode, α_n are constants depending on the mode: $\alpha_1 = 1.8751$, $\alpha_2 = 4.6941$, $\alpha_n = \pi(n - 0.5)$; k is the spring constant of the cantilever, m_c the mass of the cantilever, and m_l the mass of the medium surrounding the cantilever, e.g. liquid [6, 7].

If mass is added to the cantilever due to adsorption, the effective mass is calculated according to

$$m^* = \text{const.}(m_c + m_l + \Delta m)\,, \tag{28.7}$$

where Δm is the additional mass adsorbed. Typically, the co-moved mass of the liquid is much larger than the adsorbed mass.

Figure 28.5 clearly shows that the resonance frequency is only equal to the eigenfrequency if no damping is present. With damping, the frequency at which the peak of the resonance curve occurs is no longer identical with that at which

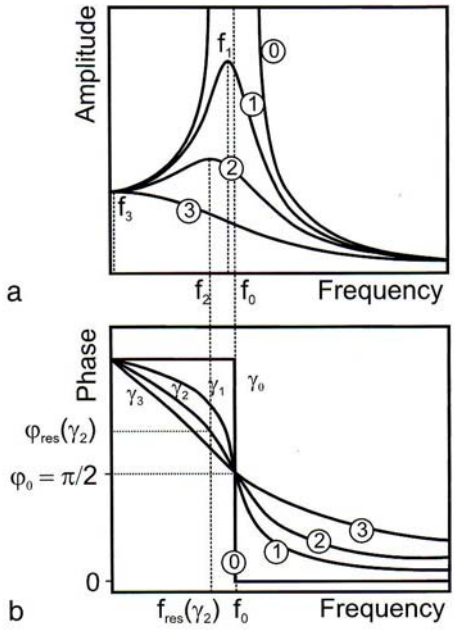

Fig. 28.5. (**a**) Resonance curve with no damping (**0**), and increasing damping (**1**)–(**3**). The undamped curve with resonance frequency f_0 shows a very high amplitude, whereas the resonance peak amplitude decreases with damping. This also involves a shift in resonance frequencies f_1 to f_3 to lower values. (**b**) Corresponding phase curves showing no damping (**0**), and increasing damping (**1**)–(**3**). The step-like phase jump at resonance of the undamped resonance gradually broadens with increasing damping

the turning point of the phase curve occurs. For example, resonance curve 2 with damping γ_2 shows its maximum amplitude at frequency f_2. The corresponding phase would be $\varphi_{\text{res}}(\gamma_2)$, which is not $\pi/2$. If direct resonance frequency tracking or a phase-locked loop is used to determine the frequency of the oscillating cantilever, then only its resonance frequency is detected, but not its eigenfrequency. Remember that the eigenfrequency, and not the resonance frequency, is required to determine mass changes.

28.1.3.3 Heat Mode

If a cantilever is coated with metal layers, thermal expansion differences in cantilever and coating layer will further influence cantilever bending as a function of temperature. This mode of operation is referred to as 'heat mode' and causes cantilever bending because of differing thermal expansion coefficients in the sensor layer and cantilever materials [2] (Fig. 28.6):

$$\Delta z = 1.25 \times (\alpha_1 - \alpha_2) \times (t_1 + t_2)/t_2^2\kappa \times l^3 P/(\alpha_1 t_1 + \alpha_2 t_2)w \,. \tag{28.8}$$

Here α_1, α_2 are the thermal expansion coefficients of the cantilever and coating materials, t_1, t_2 the material thicknesses, P is the total power generated on the cantilever, and κ a geometry parameter of the cantilever device.

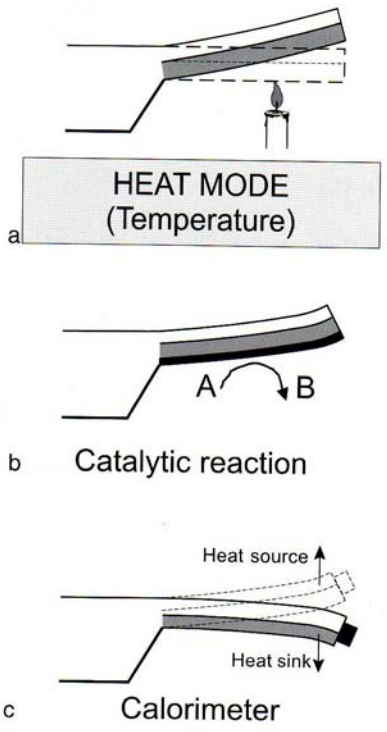

Fig. 28.6. (**a**) Cantilever heat mode. If a material with a different thermal expansion coefficient is evaporated as a thin layer onto the surface of a cantilever, then the cantilever bends when the external temperature is changed. (**b**) The heat change does not have to be generated by a change of temperature, but may also originate from heat production or drain during exothermal or endothermal reactions taking place on the cantilever surface. Exothermal processes are, for example, catalytic reactions. (**c**) If a sample is attached to the cantilever apex, a calorimetric experiment can be performed on the sample

Heat changes are either caused by external influences (change in temperature, Fig. 28.6a), occur directly on the surface by exothermal, e.g. catalytic, reactions (Fig. 28.6b), or are due to material properties of a sample attached to the apex of the cantilever (micromechanical calorimetry, Fig. 28.6c). The sensitivity of the cantilever heat mode is orders of magnitude higher than that of traditional calorimetric methods performed on milligram samples, as it only requires nanogram amounts of sample and achieves nanojoules [8] to picojoules [9, 10] of sensitivity.

These three measurement modes have established cantilevers as versatile tools to perform experiments in nanoscale science with very small amounts of material.

28.1.3.4 Other Measurement Modes

28.1.3.4.1 Photothermal Spectroscopy

When a material adsorbs photons, a fraction of energy is converted into heat. This photothermal heating can be measured as a function of the light wavelength to provide optical absorption data of the material (Fig. 28.7). The interaction of light with a bimetallic cantilever creates heat on the cantilever surface, resulting in a bending of the cantilever [11]. Such bimetallic-cantilever devices are capable of detecting heat flows due to an optical heating power of 100 pW, which is two orders of magnitude better than in conventional photothermal spectroscopy.

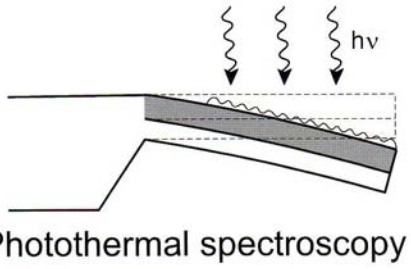

Fig. 28.7. Bending of a bimetallic cantilever due to heat production by incident photons

28.1.3.4.2 Electrochemistry

A cantilever coated with a metallic layer (measurement electrode) on one side is placed in an electrolytic medium, e.g. a salt solution, together with a metallic reference electrode, usually made of a noble metal (Fig. 28.8). Variations of the voltage between measurement and reference electrode induce electrochemical processes on the measurement electrode (cantilever), e.g. adsorption or desorption of ions from the electrolyte solution onto the measurement electrode. These processes lead to a bending of the cantilever due to changes in surface stress and in the electrostatic forces.

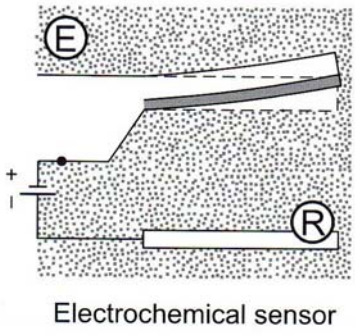

Fig. 28.8. A cantilever coated on one side with a metallic layer that is connected to a voltage source is immersed in an electrolytic fluid (**E**). The other pol e of the voltage source is connected to a reference electrode (**R**). Depending on the polarity and the magnitude of the voltage applied to the cantilever and reference electrode, ions from the electrolyte solution adsorb onto or desorb from the cantilever

28.1.3.4.3
Detection of Electrostatic and Magnetic Forces

The detection of electrostatic and magnetic forces is possible if charged or magnetic particles are deposited on the cantilever [12–14] (Fig. 28.9). If the cantilever is brought into the vicinity of electrostatic charges or magnetic particles, attractive or repulsion forces occur according to the polarity of the charges or magnetic particles present on the cantilever. These forces will result in an upwards or downwards bending of the cantilever. The magnitude of bending depends on the distribution of the charged or magnetic particles on both the cantilever and the surrounding environment according to the laws of electromagnetism.

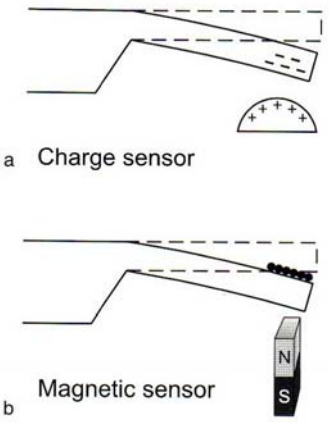

Fig. 28.9. (**a**) Cantilever bending due to electrostatic forces. (**b**) Cantilever bending due to magnetic forces

28.1.4
Cantilever Arrays

28.1.4.1
Disadvantages of Single-Cantilever Measurements

The bending response of a single cantilever is often influenced by various undesired effects, such as thermal drift and unspecific reactions taking place on the uncoated

cantilever surface, resulting in additional cantilever bending. To avoid such effects, we have introduced measurements using reference cantilevers [15], i.e. cantilever sensors that will not react with the target analyte molecules (Fig. 28.10). As the difference in signals from the reference and sensor cantilevers shows the net cantilever response, even small sensor responses can be extracted from large cantilever deflections without being predominated by undesired effects.

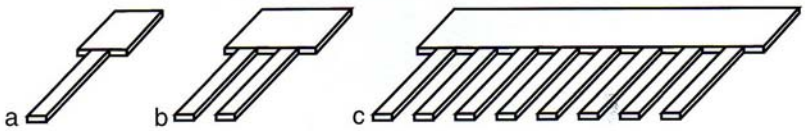

Fig. 28.10. (**a**) Single cantilever: no thermal-drift compensation is possible, both surfaces have to be chemically well-defined. One of the surfaces, e.g. the lower one, has to be passivated, otherwise the cantilever response will be convoluted with undesired effects originating from uncontrolled reactions taking place on the lower surface. (**b**) Dual cantilevers: one of them is used as the sensor cantilever (coated e.g. on the upper side with a molecule layer exhibiting affinity to the molecules to be detected), the other as the reference cantilever, coated with a passivation layer on the upper surface (exhibiting no affinity to the molecules to be detected). Thermal drifts are cancelled out if difference responses, i.e. differences in deflections of sensor and reference cantilevers are taken. Alternatively, both cantilevers are used as sensor cantilevers (sensor layer on the upper surfaces), and the lower surface is passivated. (**c**) Cantilever array: several cantilevers are used either as sensor cantilevers or as reference cantilevers so that multiple difference signals are possible simultaneously. Thermal drift is cancelled out as one surface of all cantilevers, e.g. the lower one, is left uncoated or coated with the same passivation layer

28.1.4.2 Cantilever Array Designs

Here, cantilever array designs are presented that have been used in the cantilever array sensor groups of IBM's Zurich Research Laboratory in Rüschlikon (Switzerland) and of the Institute of Physics, University of Basel (Switzerland). Accordingly, designs used by other research groups will not be discussed.

The first design in 1996 (Fig. 28.11a) consisted of a thick chip-body part (silicon, 500 μm thick, shown in grey in the figure), a doped epitaxial silicon layer for the cantilevers (1 μm thick, white), and a silicon top layer (2 μm thick, dark grey) for labeling purposes. The structures defining the chip body, the cantilevers and the top labeling layers are transferred to the silicon surfaces by means of photolithographic masks. The chips are thinned down from the lower side in an anisotropic wet-etching process using the different doping levels of the cantilevers as an etch stop. A second wet-etch step is applied from the top to release the cantilevers from the top and to etch the marks that are visible from the top. The uniformity of the cantilevers in one chip turned out to be within a few percent of the average resonance frequency. The wet-etch process steps exert considerable mechanical stress on the cantilever during production, so that defects or microcracks on some of the cantilever arrays in the wafer cannot be excluded. As all cantilevers are connected through the

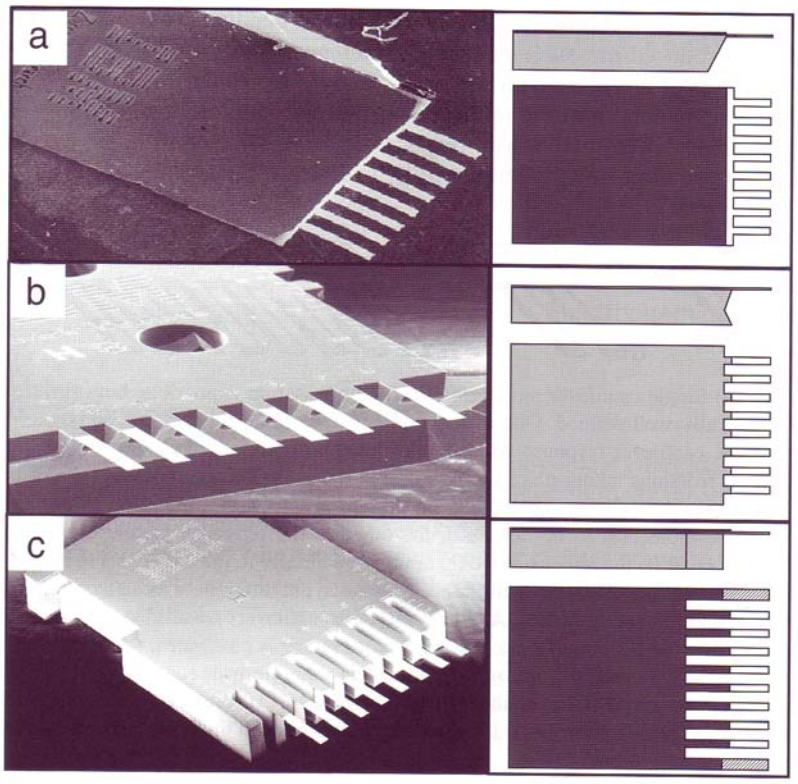

Fig. 28.11. (**a**) Cantilever array design, IBM 1996. (**b**) Cantilever array design, IBM 2000. (**c**) Cantilever array design, IBM 2003. Scanning electron micrographs on the left, side and top views on the right. The hatched area is a planned modification (not shown in the photo). Its purpose is to provide a rigid reference cantilever (full wafer thickness)

same membrane, crosstalk between responses from individual cantilevers cannot be completely excluded, although it was found to be only a few percent of the individual cantilever deflection signals.

To circumvent such crosstalk, the 2000 design was developed, which features special support structures for each cantilever, so that each cantilever is individually attached to the chip body (Fig. 28.11b). Whereas the chip body and the support structures are wet-etched from the lower side, the cantilevers are defined using dry-etching by reactive ion etching (RIE). This method produces high-aspect-ratio structures (grooves with sidewall angles larger than 85°).

To avoid time-critical wet-etching processes and the risk of damage to the cantilevers during the production process, the 2003 design relies entirely on dry-etching processes. The wall steepness has been increased to 89° by the use of improved RIE equipment, so that the etching from the lower side can also be performed by dry-etching, even if as much as 500 μm of silicon have to be etched off from the lower side. To further avoid crosstalk and to facilitate functionalization of the cantilevers, they are fixed to an extended (500-μm-long) bar-shaped structure (Fig. 28.11c).

28.1.4.3
Uniformity of Cantilever Arrays

Even if cantilever arrays consist of identical cantilevers by design, the properties might differ slightly from one cantilever to the next. For this reason, several test procedures are suggested to ascertain the uniformity of the cantilever arrays utilized in experiments.

28.1.4.3.1
Resonance-Frequency Investigation

The resonance frequency of a cantilever is basically determined by the material it consists of as well as its length, width and thickness. Measurement of the resonance frequencies in an uncoated cantilever array typically yields an absolute difference of less than 10 Hz at a typical resonance frequency of 4 kHz (1-μm-thick, 500-μm-long, 100-μm-wide cantilevers), which corresponds to a resonance frequency deviation of less than 0.25%.

28.1.4.3.2
Comparison of Responses to a Heat Pulse

One way to verify the homogeneity of gold-coated cantilevers is to observe the bending response of a bimetallic cantilever when a heat pulse is applied using a Peltier heater beneath the cantilever array. Figure 28.12 shows the response of eight cantilevers in an array to a heat pulse of 60 s duration (double arrow). The deviation in the deflection of the individual cantilevers is less than 9% of the maximum deflection observed. This gives a rough estimate of what is expected of cantilever responses in sensing experiments. However, the thermal (bimetallic) response of cantilevers may differ from the (bio-)chemical response, because the sensing layer might cause additional differences between cantilevers.

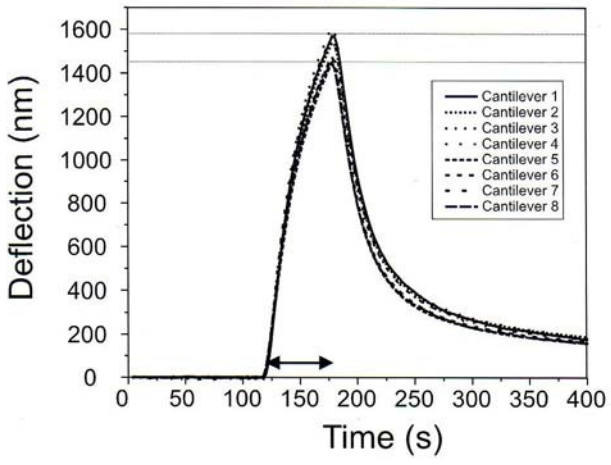

Fig. 28.12. Heat pulse of 0.71 V and 0.32 A applied for a duration of 60 s to an array of gold-coated cantilevers to test their uniformity. The *two horizontal lines* indicate smallest and largest cantilever deflections obtained from the heat pulse (data by J. Zhang, Univ. Basel, Switzerland)

28.2 Experimental Setup

28.2.1 Measurement Chamber

28.2.1.1 Designs for Gas and Liquid Environments

A measurement setup for cantilever arrays consists of four major parts: 1. the measurement chamber containing the cantilever array, 2. an optical or piezoresistive system to detect the cantilever deflection (e.g. laser sources, collimation lenses and a position-sensitive detector (PSD), 3. electronics to amplify, process and acquire

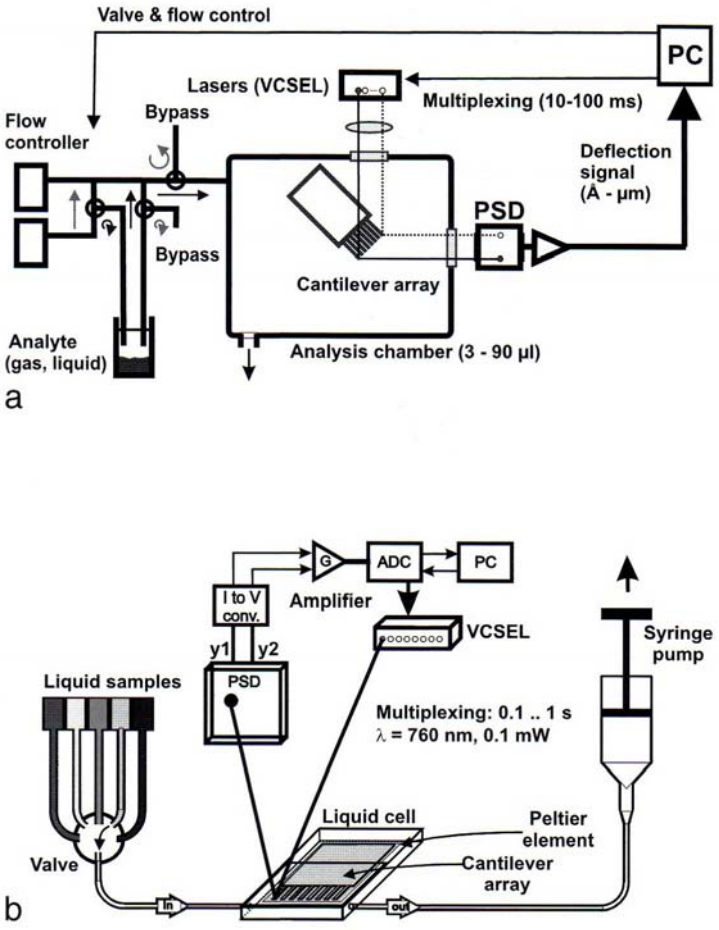

Fig. 28.13. Schematic of measurement setups for (**a**) a gaseous (artificial nose) and (**b**) a liquid environment (biochemical sensor)

the signals from the PSD, and 4. a gas- or liquid-handling system to reproducibly inject samples into the measurement chamber and purge the chamber.

Figure 28.13 shows the schematic setup of the experiments performed in (a) a gaseous and (b) a liquid (biochemical) environment. The cantilever sensor array is located in an analysis chamber of 3–90 µl in volume, which has inlet and outlet ports for gases or liquids. The cantilever deflection is determined by means of an array of eight vertical-cavity surface-emitting lasers (VCSELs) arranged at a linear pitch of 250 µm that emit at a wavelength of 760 nm into a narrow cone of 5 to 10°.

The light of each VCSEL is collimated and focused onto the apex of the corresponding cantilever by a pair of achromatic doublet lenses, 12.5 mm in diameter. This size was selected so that all eight laser beams pass through the lenses close to its center in order to minimize scattering, chromatic and spherical aberration artifacts. The light is then reflected off the gold-coated surface of the cantilever and hits the surface of a PSD. PSDs are light-sensitive photo-potentiometer-like devices that produce photocurrents at two opposing electrodes. The magnitude of the photocurrents linearly depends on the distance of the impinging light spot from the electrodes. Thus the position of an incident light beam can be determined with micrometer precision. The photocurrents are transformed into voltages and amplified in a preamplifier (see Fig. 28.14). As only one PSD is used, the eight lasers cannot be switched on simultaneously. Therefore, a time-multiplexing procedure is used to switch the lasers on and off sequentially at typical intervals of 10–100 ms (see Fig. 28.15). The resulting

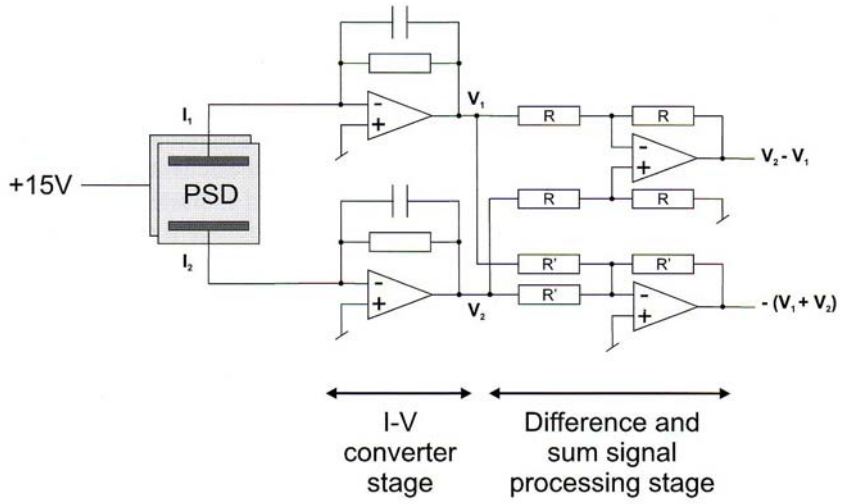

Fig. 28.14. Schematic circuit drawing of a current-to-voltage converter and preamplifier that produces difference and sum signals. The PSD is biased at +15 V to decrease its capacitance and enhance its response. The photocurrents I_1 and I_2 are fed into a current-to-voltage (I–V) converter stage to obtain voltages V_1 and V_2. These are further processed to yield a difference signal $V_2 - V_1$, which is used to measure cantilever deflection, and a sum signal $V_1 + V_2$, which measures the total intensity of light on the PSD and serves as a reference value to keep the intensity of the VCSELs constant (courtesy of A. Tonin, Univ. Basel, Switzerland)

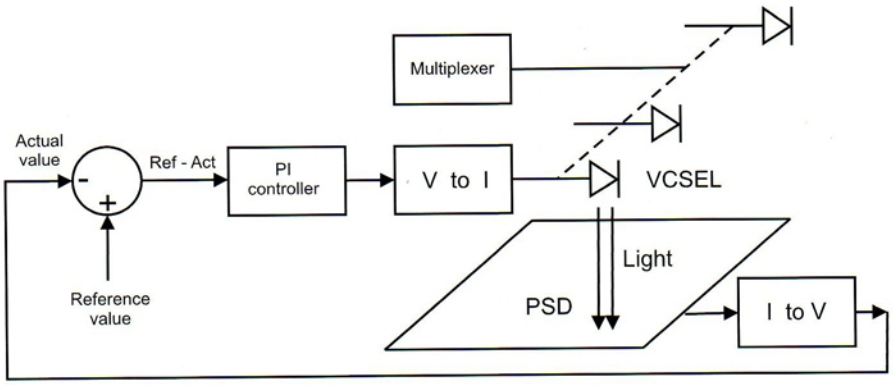

Fig. 28.15. Schematic circuit drawing of the VCSEL driver to switch on and off the eight VCSELs and to keep their light intensity constant. The light of a VCSEL impinges on the PSD and produces photocurrents $I_{1,2}$ that are converted into voltages $V_{1,2}$ in the preamplifier (I to V). The sum signal $V_1 + V_2$ is fed into a voltage comparator, which compares the actual value of the sum signal with a preset reference value. The difference between reference and actual value is then used as input to a PI controller that regulates the current to drive the VCSELs at constant intensity (V to I). A multiplexer switches all eight VCSELs on and off sequentially (courtesy of A. Tonin, Univ. Basel, Switzerland)

deflection signal is digitized and stored together with time information on a personal computer (PC), which also controls the multiplexing of the VCSELs as well as the switching of the valves and mass flow controllers used for setting the composition ratio of the analyte mixture.

The measurement setup for liquids (Fig. 28.13b) consists of a poly-etheretherketone (PEEK) liquid cell, which contains the cantilever array and is sealed by a viton O-ring and a glass plate. The VCSELs and the PSD are mounted on a metal frame around the liquid cell. After preprocessing the position of the deflected light beam in a current-to-voltage converter and amplifier stage (Fig. 28.14), the signal is digitized in an analog-to-digital converter and stored on a PC. The liquid cell is equipped with inlet and outlet ports for liquids. They are connected via 0.18 mm of i.d. teflon tubing to individual thermally-equilibrated glass containers, in which the biochemical liquids are stored. A six-position valve allows the inlet to the liquid chamber to be connected to each of the liquid-sample containers separately. The liquids are pulled (or pushed) through the liquid chamber by means of a syringe pump connected to the outlet of the chamber. A Peltier element is situated very close to the lumen of the chamber to allow temperature regulation within the chamber. The entire experimental setup is housed in a temperature-controlled box regulated with an accuracy of 0.01 K to the target temperature.

28.2.2 Cantilever Functionalization

To serve as sensors, cantilevers have to be coated with a sensor layer that is either highly specific, i.e. is able to recognize target molecules in a key-lock process,

or partially specific, so that the sensor information from several cantilevers yields a pattern that is characteristic of the target molecules.

To provide a platform for specific functionalization, the upper surface of these cantilevers is generally coated with 2 nm of titanium and 20 nm of gold, which yields a reflective surface and an interface for attaching functional groups of probe molecules, e.g. for anchoring molecules with a thiol group to the gold surface of the cantilever. Such thin metal layers are believed not to contribute significantly to the bending due to surface-stress changes, because the temperature is kept constant. Many examples of molecular adsorption on cantilevers are described in the literature, for example, the adsorption of alkyl thiols on gold [16, 17], the detection of mercury vapor and relative humidity [18], dye molecules [19], monoclonal antibodies [20], sugar and proteins [21], solvent vapors [22–24], fragrance vapors [25], as well as the pH-dependent response of carboxy-terminated alkyl thiols [26], label-free DNA hybridization detection [27, 28], and biomolecular recognition of proteins relevant in cardiovascular diseases [29].

28.2.2.1
Functionalization Methods

There is a large variety of both simple and more advanced methods to coat a cantilever with material. The requirement is to develop a fast, reproducible and reliable method for the functionalization of one or both of the surfaces of a cantilever separately.

28.2.2.1.1
Simple Methods

Obvious methods to coat a cantilever include thermal or electron-beam-assisted evaporation of material, electro-spray or other deposition methods. The disadvantage of these methods is that inherently they do not provide sufficient resolution to coat individual cantilevers in an array, unless shadow masks are used. Such masks need to be accurately aligned with the cantilever structures, which is a time-consuming process.

Other methods to coat cantilevers use manual placement of particles onto the cantilever [2,5,8,19,30], which requires skillful handling of tiny samples. Cantilevers can also be coated by directly pipetting solutions of the probe molecules onto the cantilevers [22], or by means of air-brush spraying and shadow masks to coat the cantilevers separately [24].

All these methods only have limited reproducibility if a larger number of cantilever arrays has to be coated. As manual alignment is required, these methods are very time-consuming.

28.2.2.1.2
Microfluidic Networks

A step towards reliable and reproducible coating procedures is achieved by the use of microfluidic networks (μFN) [31]. μFN are structures of channels and wells, etched

several tens to hundreds of micrometers deep into silicon-wafers. The wells can be filled easily using a laboratory pipette, so that the fluid with the probe molecules to be attached to the cantilever is guided through the channels towards openings at a pitch matched to the distance between individual cantilevers in the array (see Fig. 28.16).

The cantilever array is then approached to the opening by means of an x-y-z positioner, with an accuracy of better than 10 μm, and introduced into the open channels of the μFN that are filled with a solution of the probe molecules. The incubation of the cantilever array in the channels of the μFN takes from a few seconds (self-assembly of alkanethiol monolayers) to several tens of minutes (coating with protein solutions). To prevent evaporation of the solutions, the channels are covered by a slice of PDMS. In addition, the microfluidic network can be placed in a container filled with saturated vapor of the solvent used for the probe molecules. The obtained functional layers on the cantilevers are of good and reproducible quality, and the coating process is considerable faster than with the above-described simple techniques.

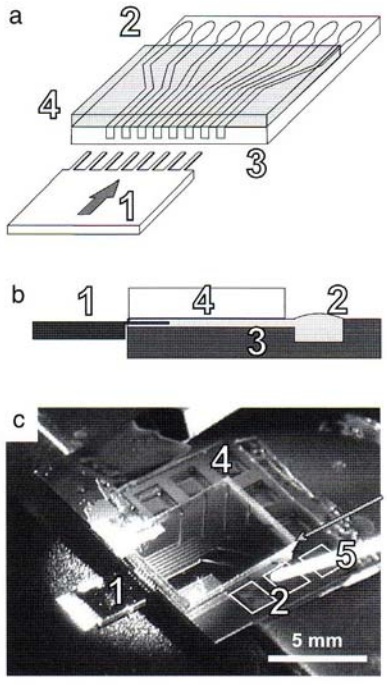

Fig. 28.16. Microfluidic network for functionalization of cantilever arrays. (**a**) Schematic, (**b**) side view, (**c**) photo of the actual device. (**1**) Cantilever array, (**2**) reservoir wells, (**3**) microfluidic network with channels, (**4**) PDMS cover to avoid evaporation of the liquid, (**5**) pipette to fill the reservoir well. Figure courtesy of A. Bietsch, Univ. Basel, Switzerland

28.2.2.1.3
Array of Dimension-Matched Glass Capillaries

As the positioning of the cantilever array relative to the μFN still requires manual alignment, we have developed a device in which the cantilever array is placed rigidly

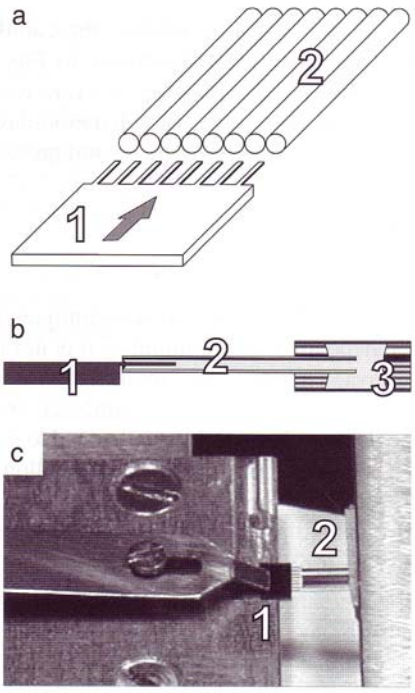

Fig. 28.17. Setup for cantilever array functionalization using an array of dimension-matched microcapillaries. (**a**) Schematic, (**b**) side view, (**c**) photo. (**1**) Cantilever array, (**2**) glass capillaries, (**3**) tubing with liquid reservoir in a larger piece of tubing to compensate for liquid losses due to evaporation. Figure courtesy of A. Bietsch, Univ. Basel, Switzerland

in a fit with an accuracy of better than 50 μm and fixed with a clamp (Fig. 28.17). Because the μFN needs to be cleaned thoroughly after each functionalization process, we replaced the μFN channels by an array of dimension-matched disposable glass capillaries. The outer diameter of the glass capillaries is 240 μm so that they can be placed neatly next to each other to accommodate the pitch of the cantilevers in the array (250 μm). Their inner diameter is 150 μm, providing sufficient room to insert the cantilevers (width: 100 μm) safely.

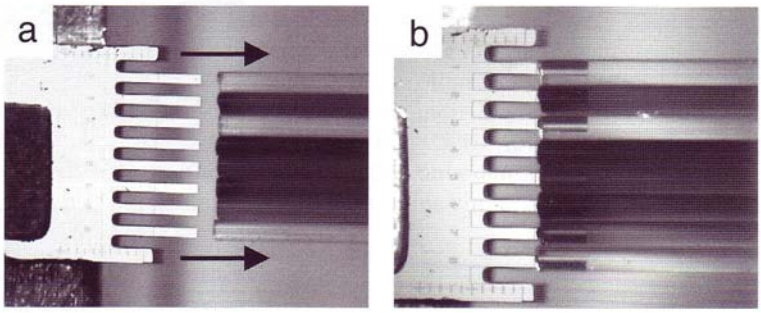

Fig. 28.18. Cantilever array (**a**) before and (**b**) after insertion into the open ends of an array of microcapillaries. The *different shades of grey* in the capillaries are due to the filling of the capillaries with various dyes. Note that the capillaries can only be moved until they touch the wafer-thick finger structures (see Fig. 28.11c). Courtesy of A. Bietsch, Univ. Basel, Switzerland

A detailed view of how the cantilevers in an array are inserted into an array of glass capillaries is shown in Fig. 28.18. This method has been successfully applied for the deposition of a variety of materials onto cantilevers, e.g. for polymer solutions [24], self-assembled monolayers [26], thiol-functionalized single-stranded DNA oligonucleotides [28], and protein solutions [29].

28.2.2.1.4 Inkjet Spotting

Even if the capillary-array technique yields reliable and reproducible layers that can be deposited within minutes, it is not ideal for coating a large number of cantilever arrays. Therefore, we applied the inkjet printing technique to establish a rapid and general method to coat cantilever arrays [32, 33] (Fig. 28.19). This technique is scalable to large arrays and can also coat arbitrary structures in noncontact manner.

An *x*-*y*-*z* positioning system allows a sharp nozzle (capillary diameter: 70 μm) to be positioned with an accuracy of approx. 10 μm over a cantilever. Individual droplets (diameter: 60–80 μm, volume 0.1–0.3 nl) can be dispensed individually by use of a piezo-driven ejection system in the inkjet nozzle. When the droplets are

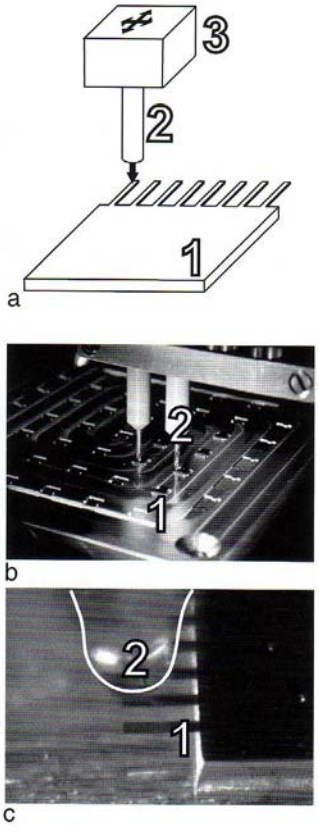

Fig. 28.19. Cantilever array functionalization by inkjet spotting. (**a**) Schematic, (**b**) photo of the actual device, (**c**) closeup. (**1**) Cantilever array, (**2**) inkjet nozzle, (**3**) *x*-*y*-*z* positioning unit. Courtesy of A. Bietsch, Univ. Basel, Switzerland

spotted with a pitch smaller than 0.1 mm, they merge and form continuous films. By adjusting the number of droplets deposited on cantilevers, the resulting film thickness can be controlled precisely.

The inkjet-spotting technique allows a cantilever to be coated within seconds and yields very homogeneous, reproducibly deposited layers of well-controlled thickness. Successful coating of self-assembled alkanethiol monolayers, polymer solutions, self-assembled DNA single-stranded oligonucleotides [33], and protein layers has been demonstrated.

In conclusion, inkjet spotting has turned out to be a very efficient method for functionalization that is not restricted to cantilevers, but can easily and rapidly coat even arbitrarily shaped sensors reproducibly and reliably [34, 35].

28.2.2.2
Functionalization Procedure

28.2.2.2.1
Polymer-Coated Cantilever Arrays

Polymer layers were deposited on a gold-coated cantilever array by inkjet spotting. Various commercial polymers were dissolved in solvents (5 mg/ml). Eight droplets of solution were dispensed onto the upper surface of one of the cantilevers of the array by inkjet spotting [32, 33], allowed to dry and form a homogeneous polymer layer of a few hundred nanometers in thickness. The following polymers were used: CMC: carboxymethylcellulose sodium salt in water (all concentrations 5 mg/ml); PEG: polyethylene glycol 6000 in water; PEI: polyethyleneimine in water; PSS: poly(sodium 4-styrene sulfonate), MW 70,000 in water; PAAM: poly(allylamine hydrochloride), MW 15,000 in water; PVP: poly(2-vinylpyridine) standard, MW 64,000 in ethanol; PVA: polyvinylalcohol 10-98 in dimethylsulfoxide; PMMA: polymethymethacrylate, MW 15,000 in methyl-isobutyl-ketone.

28.2.2.2.2
DNA-Coated Cantilever Arrays

For measurements in the liquid phase, functional monolayers were deposited by self-assembly of thiolated molecule layers, e.g. DNA oligonucleotide layers for hybridization experiments in liquid. Various oligonucleotide layers were applied in parallel and under identical conditions to the individual cantilever sensors by means of microcapillaries (see Fig. 28.17 and Fig. 28.18), filled with a 40-μM solution of 3′- or 5′-thiolated probe DNA in triethyl ammonium acetate buffer for 20 min. The coated arrays were rinsed in sodium saline citrate (ssc) 5× buffer and dried in nitrogen [28].

28.3 Measurements

Measurements using cantilever array sensors can either be highly specific to detect molecules that match a receptor site on the cantilever coating or partially specific,

i.e. several cantilever sensors respond to the presence of a vapor, but only the pattern of responses of all eight cantilevers contains sufficient information to characterize a sample vapor. In the following, two experiments are presented. The first demonstrates the partial sensitivity of polymer-coated cantilevers as a kind of "artificial nose" [36] in a gaseous environment, the other shows the high specificity of a DNA hybridization recognition reaction in liquid.

28.3.1 Artificial Nose for Detection of Perfume Essences

A cantilever array consisting of eight differently coated cantilevers can be employed as an "artificial nose" to characterize vapors. The key elements of an artificial nose [36] are 1. chemical sensors composed of a physical transducer and a chemical interface layer or a receptor domain with partial specificity; 2. an appropriate pattern-recognition system to recognize simple or complex odors (pattern classifier), and 3. a sampling system to reproducibly perform measurements. The sensor array is exposed to the same sample, and produces individual responses, as well as a pattern of responses.

The main advantage of an artificial nose is that it is reproducible, does not wear out, and can be placed in environments that are harmful to humans.

Here we use polymer-coated cantilevers as chemical sensors prepared as described above. Detection of vapors proceeds via diffusion of the vapor molecules into the polymer, resulting in a swelling of the polymer and bending of the cantilever. The bending is specific to the interaction between the solvent vapor and polymer time- and magnitude-wise. To demonstrate the capability of the cantilever array artificial nose, we injected vapor (20 ml/min) from the headspace above 0.1 ml of ethanolic solution of perfume essence samples (lemon, wood, flower; main components: ethanol 35%, water 14%, dipropylene glycol 50%, fragrances $< 1\%$) in a stream of dry nitrogen. Figure 28.20 shows the deflection traces from eight polymer-coated cantilevers upon injection of perfume essence vapor during 60 s (starting at $t = 100$ s). The cantilever responses of three samples are shown (two wood essence and one lemon essence sample).

A "fingerprint" of the perfume essence sample is generated by reducing the deflection curves of all eight cantilevers to a discrete set of cantilever amplitudes at several points in time, e.g. at 110 s, 130 s, and 150 s. This yields in total $8 \times 3 = 24$ cantilever deflection amplitudes that account for a measurement data set.

This data set is then evaluated using principal-component-analysis (PCA) techniques [37], which extracts the most dominant deviations in the responses for the various perfume essence vapors. The largest differences in signal amplitudes of the fingerprint patterns are plotted in a two-dimensional graph, whereby an individual measurement (i.e. a set of 24 cantilever magnitudes) represents a single point in the PCA space. The axes refer to projections of the multidimensional datasets into two dimensions (principal components). This procedure is targeted at maximum distinction performance between analytes, i.e. several measurements of the same analyte should yield a cluster in principal-component space, whereas measurements of differing analytes should produce well-separated clusters of measurements.

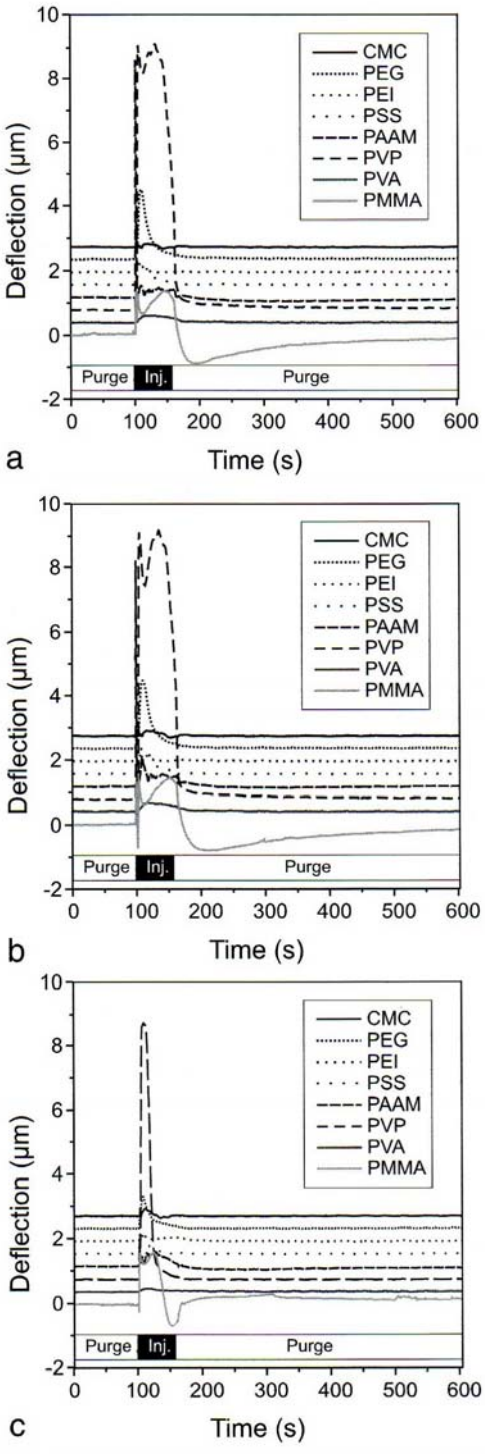

Fig. 28.20. Bending patterns of polymer-coated cantilever sensors upon exposure to perfume essence vapor. (**a**) Wood flavor (first sample), (**b**) wood flavor (second sample), (**c**) lemon flavor. "Purge" means flushing the measurement chamber with dry nitrogen gas at a rate of 20 ml/min, "Inj." denotes the injection of dry nitrogen gas saturated with the vapor from the headspace of a vial filled with 100 µl of ethanolic solution of perfume essence. The cantilever deflection responses are offset for clarity reasons

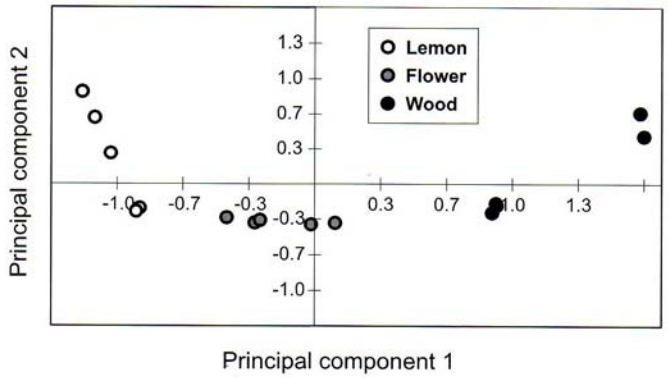

Fig. 28.21. PCA plot of perfume essence samples. Measurements of flower, wood and lemon perfume essences reveal three clearly distinguishable clusters

The PCA evaluation of the cantilever-sensor response curves is shown in Fig. 28.21. Clear clustering is observed for the perfume essences tested, demonstrating the successful recognition, as well as the selectivity of the method. However, the "artificial nose" can only recognize sample vapors that have been measured before. Therefore, it is a characterization rather than a chemical-analysis tool.

28.3.2 Label-Free DNA Hybridization Detection

The main advantage of cantilever array sensors is the possibility that measurements of differences in the responses of sensor and reference cantilevers can be evaluated. Measuring the deflection of only one cantilever will yield misleading results that might give rise to an incorrect interpretation of the cantilever-deflection trace [38].

Therefore, at least one of the cantilevers (the sensor cantilever) is coated with a sensitive layer that exhibits an affinity to the molecules to be detected, whereas other cantilevers are coated with a molecular layer that does not show an affinity to them (reference cantilevers). The biochemical system to be investigated here involves a DNA hybridization experiment in liquid using a thiolated 12-mer oligonucleotide sequence from the Bio B biotin synthetase gene (EMBL accession number: J04423). We selected three surface-bound probes, Bio B1 (5′-SH-C_6-ACA TTG TCG CAA-3′, C_6 is a spacer), Bio B2 (5′-SH-C_6-TGC TGT TTG AAG-3′) and Bio B6 (5′-SH-C_6-TCA GGA ACG CCT-3′), which are immobilized by thiol binding onto the gold-coated upper surface of a cantilever in an array (Fig. 28.22a).

The target complements are called Bio B1C, B2C and B6C are diluted in 5x ssc buffer at 100 pM concentration. Upon injection of the matching sequence to Bio B1, i.e. Bio B1C, the sensor cantilever coated with Bio B1 will bend, whereas the reference cantilever coated with Bio B2 will not bend (Fig. 28.22b). After thorough rinsing with an unbinding agent, the cantilever coated with Bio B1 will bend back to its initial position (Fig. 28.22c). The bending is due to the formation of surface stress during the hybridization process because of steric crowding (double-stranded DNA requires more space than single-stranded DNA).

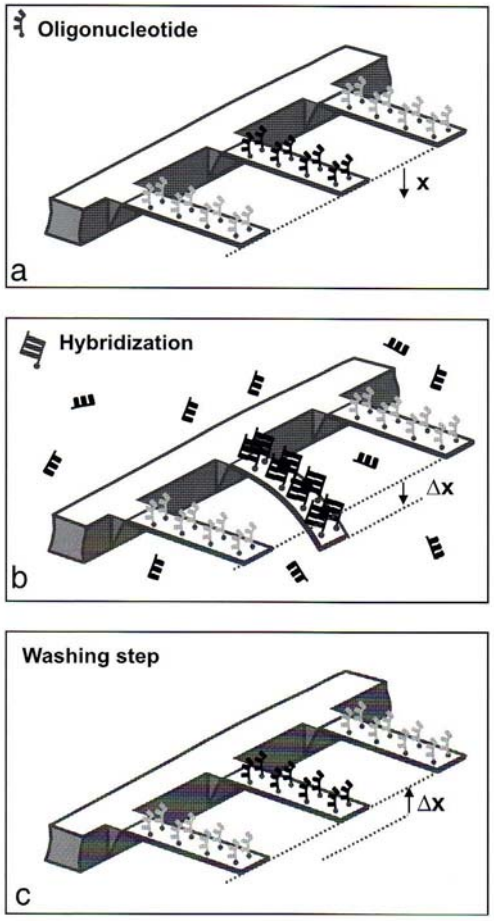

Fig. 28.22. Schematic of the cantilever array DNA hybridization sensor. (**a**) Each cantilever is functionalized with a self-assembled monolayer of thiolated oligonucleotides. (**b**) Upon injection of the complementary sequence to the oligonucleotide sequence shown in the middle, hybridization takes place and the cantilever bends downwards. (**c**) After thorough rinsing with an unbinding agent, the cantilever in the middle returns to its initial position. The schematics are courtesy of Jürgen Fritz, currently at the International University of Bremen, Germany

The actual experiment proceeds as follows (see Fig. 28.23a): First, the liquid cell with the functionalized cantilever array is filled with ssc buffer. After a stable base line has been achieved, ssc buffer is injected after 4 min for 3 min. The cantilevers deflect, but once the injection is over, a stable baseline is reached again. At 18 min, the target Bio B1C is injected, which is supposed to hybridize with the Bio B1 probe, but not with the Bio B2 or the Bio B6 probe. Both cantilevers deflect, but the deflection magnitude of the Bio B1-coated cantilever is larger than that of the Bio B2-coated cantilever. Finally, at 37 min, ssc buffer is injected again and a stable baseline is reached. From the deflection data shown in Fig. 28.23a, it is clear that no conclusive result can be obtained from individual cantilever responses only, as both the sensor and the reference cantilevers bend. However, a clear 20 nm deflection signal is observed when calculating the difference in deflection responses from probes Bio B1 (sensor) and reference Bio B2 (Fig. 28.23b), or the difference in deflection responses from probes Bio B1 and reference Bio B6. The differential deflection magnitudes obtained are 25 nm (B1–B2) or 30 nm (B1–B6), respectively.

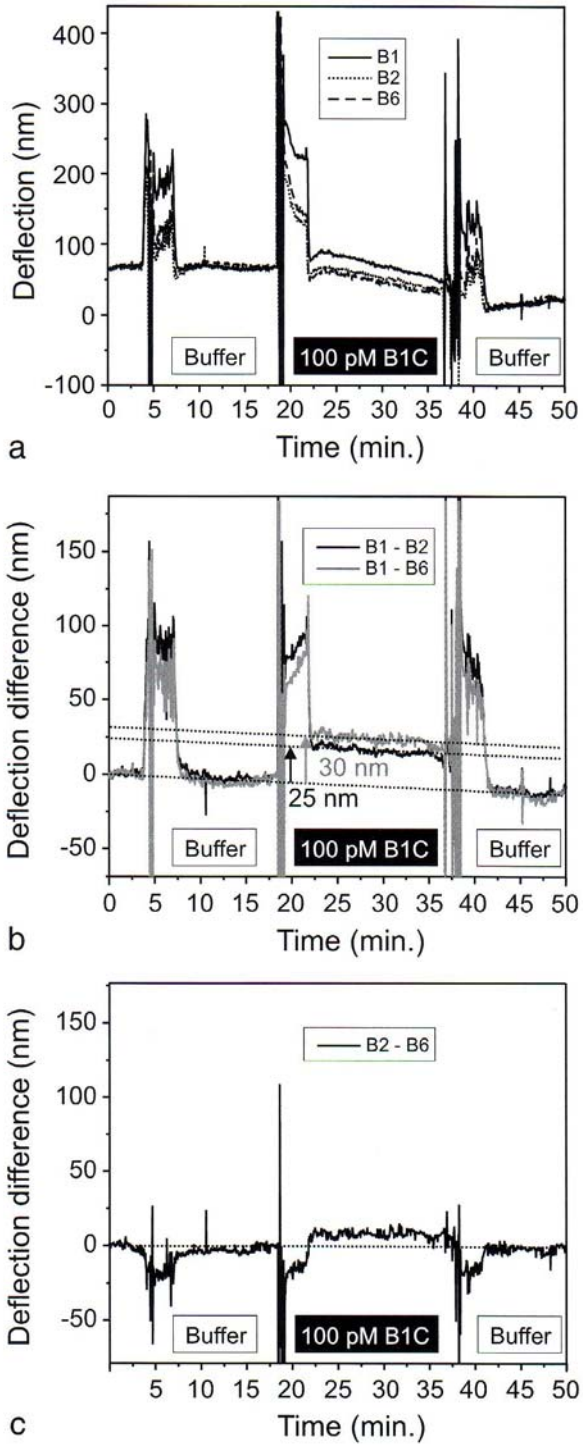

Fig. 28.23. (**a**) Deflection traces of sensor (functionalized with DNA oligonucleotide sequence Bio B1) and reference cantilevers (functionalized with DNA oligonucleotide sequences Bio B2 and Bio B6, respectively). (**b**) Differences B1 to B2 and B1 to B6 of the bending responses of the sensor cantilever B1 and the reference cantilevers B2 and B6. The *dotted lines* are guides to the eye. The hybridization of B1 with B1C yields a difference signal of 25 (B1–B2) or 30 nm (B1–B6). (**c**) Difference in responses of the two reference probes. B2–B6 only yields a small signal of 5 nm. "Buffer" indicates flushing the cell with 5x ssc buffer; "100 pM B1C" means injection of the complement to Bio B1 at a concentration of 100 pM in ssc buffer. Data courtesy of J. Zhang, University of Basel, Switzerland

The difference in deflection responses between two reference cantilevers yields no signal or only a very small signal that can be attributed to some unspecific binding of B1C to one of the reference probes, supposedly to B2, as the difference B2–B6 yields a positive signal of less than 5 nm, see Fig. 28.23c. We conclude that it is absolutely mandatory to use at least two cantilevers in an experiment, a reference cantilever and a sensor cantilever, to be able to cancel out undesired artifacts such as thermal drift or unspecific adsorption.

28.4 Applications and Outlook

The field of cantilever sensors has been very active in recent years [39–41]. Chief topics published 2003 and 2004 in the literature include the following studies: fabrication of silicon, piezoresistive [42, 43] or polymer [44] cantilevers, detection of vapors and volatile compounds, e.g. mercury vapor [45], HF vapor [46,47], chemical vapors [48,49], as well as the development of gas sensors utilizing the piezoresistive method [50]. Pd based sensors for hydrogen [51], deuterium and tritium [52, 53] have been reported, as well as sensors based on hydrogels [54–57] or zeolites [58]. A humidity sensor is suggested in [59]. Many articles investigate the topics of detection of explosives [60–65], pathogens [66], nerve agents [67], viruses [68], bacteria, e.g. *E. coli* [69–71], and pesticides like dichlorodiphenyltrichloroethane (DDT) [72]. Issues of detection of environmental pollutants are discussed in [73, 74]. A chemical vapor sensor based on the bimetal technique is described in [75]. Several papers study the mechanism of static cantilever bending [76–78] and how the transduction can be improved by surface modification of the sensor layer on the cantilever [79,80], or how its properties can be improved [81–83]. In two publications, electrochemical redox reactions are measured with cantilevers [84, 85]. A large number of papers are focused on biochemical applications using cantilevers, e.g. to detect DNA [86–89], proteins [90,91], prostate-specific antigen (PSA) [92], peptides using antibodies [93, 94] and living cells [95]. Most groups use the static deflection mode for measurements in liquids, whereas others use piezoresistive cantilevers [96] or the heat mode (calorimeter biosensor) [97]. The understanding of the chemistry [98] and the mechanism [99] of biosensing is of big importance, as is a strategy to improve the transduction mechanism [100]. Medical applications involve diagnostics [101], drug discovery [102] and detection of substances like glucose [103, 104]. Mass measurement in dynamic mode is investigated in a variety of publications, e.g. down to the attogram regime in ultra-high vacuum [105] using Doppler vibrometer readout of the oscillation [106]. Several authors study the modeling of resonant sensors [107–114] and exploit higher modes [115], as well as torsional or lateral resonance modes for improved mass sensing in dynamic mode [116, 117]. To improve the oscillation [118], the quality factor can be enhanced electronically [119, 120]. Effects of temperature and pressure on the oscillation should also be taken into account [121]. Other researchers use piezoresonators integrated into the cantilever structure [122].

Ellipsometry combined with cantilever readouts has been suggested [123] as a combined technique. Cantilevers have been used to calibrate AFM cantilevers [124, 125]. Nanowire electrodes attached to cantilevers in an array can be used for local

multiprobe resistivity measurements [126]. Two-dimensional microcantilever arrays have been proposed for multiplexed biomolecular analysis [127, 128].

We conclude that cantilever-sensor array techniques are very powerful and highly sensitive tools to study physisorption and chemisorption processes, as well as to determine material-specific properties such as heat transfer during phase transitions. Experiments in liquid environments have provided new insight on such complex biochemical reactions as the hybridization of DNA or molecular recognition in antibody/antigen systems or proteomics. Future developments point towards technological applications, e.g. to finding new ways to characterize real-world samples such as clinical samples. For example, the development of medical diagnosis tools requires the improvement of the sensitivity of a large number of genetic tests to be performed with small amounts of single donor-blood or body-fluid samples. On the other hand, from a scientific point of view, the challenge lies in optimizing cantilever sensors to improve their sensitivity to the ultimate limit: the detection of individual molecules.

Acknowledgements. We thank R. McKendry (University College London, London, U.K.), J. Zhang, A. Bietsch, V. Barwich, M. Ghatkesar, F. Huber, J.-P. Ramseyer, A. Tonin, H.R. Hidber, E. Meyer and H.-J. Güntherodt (University of Basel, Basel, Switzerland) for valuable contributions and discussions, as well as U. Drechsler, M. Despont, H. Schmid, E. Delamarche, H. Wolf, R. Stutz, R. Allenspach, and P.F. Seidler (IBM Research, Zurich Research Laboratory, Rüschlikon, Switzerland). This project was partially funded by the National Center of Competence in Research in Nanoscience (Basel, Switzerland), the Swiss National Science Foundation and the Commission for Technology and Innovation (Bern, Switzerland).

References

1. Binnig G, Quate CF, Gerber C (1986) Phys Rev Lett 56:930
2. Gimzewski JK, Gerber C, Meyer E, Schlittler RR (1994) Chem Phys Lett 217:589
3. Stoney GG (1909) Proc R Soc London Ser A 82:172
4. Thundat T, Warmack RJ, Chen GJ, Allison DP (1994) Appl Phys Lett 64:2894
5. Berger R, Lang HP, Gerber C, Gimzewski JK, Fabian JH, Scandella L, Meyer E, Güntherodt H-J (1998) Chem Phys Lett 294:363
6. Greenspoon JE (1961) J Acoust Soc America 33:1485
7. Zhang J, O'Shea S (2003) Sens Actuators B 94:65
8. Berger R, Gerber C, Gimzewski JK, Meyer E, Güntherodt H-J (1996) Appl Phys Lett 69:40
9. Bachels T, Schäfer R (1999) Chem Phys Lett 300:177
10. Bachels T, Tiefenbacher F, Schäfer R (1999) J Chem Phys 110:10008
11. Barnes JR, Stephenson RJ, Welland ME, Gerber C, Gimzewski JK (1994) Nature 372:79
12. Puers R, Lapadatu D (1996) Sens Actuators A 56:203
13. Huang JM, Liew KM, Wong CH, Rajendran S, Tan MJ, Liu AQ (2001) Sens Actuators A 93:273
14. Fricke J, Obermaier C (1993) J Micromech Microeng 3:100
15. Lang HP, Berger R, Andreoli C, Brugger J, Despont M, Vettiger P, Gerber C, Gimzewski JK, Ramseyer J-P, Meyer E, Güntherodt H-J (1998) Appl Phys Lett 72:383
16. Berger R, Delamarche E, Lang HP, Gerber C, Gimzewski JK, Meyer E, Güntherodt H-J (1997) Science 276:2021
17. Berger R, Delamarche E, Lang HP, Gerber C, Gimzewski JK, Meyer E, Güntherodt H-J (1998) Appl Phys A 66:S55

18. Wachter EA, Thundat T (1995) Rev Sci Instrum 66:3662
19. Scandella L, Binder G, Mezzacasa T, Gobrecht J, Berger R, Lang HP, Gerber C, Gimzewski JK, Koegler JH, Jansen JC (1998) Micropor Mesopor Mater 21:403
20. Raiteri R, Nelles G, Butt H-J, Knoll W, Skladal P (1999) Sens Actuators B 61:213
21. Moulin AM, O'Shea SJ, Welland ME (2000) Ultramicroscopy 82:23
22. Lang HP, Berger R, Battiston FM, Ramseyer J-P, Meyer E, Andreoli C, Brugger J, Vettiger P, Despont M, Mezzacasa T, Scandella L, Güntherodt H-J, Gerber C, Gimzewski JK (1998) Appl Phys A 66:S61
23. Lang HP, Baller MK, Berger R, Gerber C, Gimzewski JK, Battiston FM, Fornaro P, Ramseyer J-P, Meyer E, Güntherodt H-J (19999) Anal Chim Acta 393:59
24. Baller MK, Lang HP, Fritz J, Gerber C, Gimzewski JK, Drechsler U, Rothuizen H, Despont M, Vettiger P, Battiston FM, Ramseyer J-P, Fornaro P, Meyer E, Güntherodt H-J (2000) Ultramicroscopy 82:1
25. Battiston FM, Ramseyer J-P, Lang HP, Baller MK, Gerber C, Gimzewski JK, Meyer E, Güntherodt H-J (2001) Sens Actuators B 77:122
26. Fritz J, Baller MK, Lang HP, Strunz T, Meyer E, Güntherodt H-J, Delamarche E, Gerber C, Gimzewski JK (2000) Langmuir 16:9694
27. Fritz J, Baller MK, Lang HP, Rothuizen H, Vettiger P, Meyer E, Güntherodt H-J, Gerber C, Gimzewski JK (2000) Science 288:316
28. McKendry R, Zhang J, Arntz Y, Strunz T, Hegner M, Lang HP, Baller MK, Certa U, Meyer E, Güntherodt H-J, Gerber C (2002) Proc Nat Acad Sci USA 99:9783
29. Arntz Y, Seelig JD, Lang HP, Zhang J, Hunziker P, Ramseyer J-P, Meyer E, Hegner M, Gerber C (2003) Nanotechnology 14:86
30. Berger R, Gerber C, Lang HP, Gimzewski JK (1997) Microelectron Eng 35:373
31. Wolf H, Juncker, D, Michel B, Hunziker P, Delamarche E (2004) Biosens Bioelectron 10:1193
32. Bietsch A, Hegner M, Lang HP, Gerber C (2004) Langmuir 20:5119
33. Bietsch A, Zhang J, Hegner M, Lang, HP, Gerber C (2004) Nanotechnology 15:873
34. Lange D, Hagleitner C, Hierlemann A, Brand O, Baltes H (2002) Anal Chem 74:3084
35. Savran CA, Burg TP, Fritz J, Manalis SR (2003) Appl Phys Lett 83:1659
36. Gardner JW, Bartlett PN (1992) Sensors and Sensory Systems for an Electronic Nose. Kluwer, Dordrecht
37. Timm, NH (2002) Springer Texts in Statistics – Applied Multivariate Analysis. Springer, Berlin Heidelberg New York
38. Lang HP, Hegner M, Meyer E, Gerber C (2002) Nanotechnology 13:R29
39. Ziegler C (2004) Anal Bioanal Chem 379:946
40. Lavrik NV, Sepaniak MJ, Datskos PG (2004) Rev Sci Instrum 75:2229
41. Majumdar A (2002) Disease Markers 18:167
42. Tang YJ, Fang J, Yan XD, Ji HF (2004) Sens Actuators B 97:109
43. Forsen E, Nilsson SG, Carlberg P, Abadal G, Perez-Murano F, Esteve J, Montserrat J, Figueras E, Campabadal F, Verd J, Montelius L, Barniol N, Boisen A (2004) Nanotechnology 15:S628
44. McFarland AW, Poggi MA, Bottomley LA, Colton JS (2004) Rev Sci Instrum 75:2756
45. Rogers B, Manning L, Jones M, Sulchek T, Murray K, Beneschott B, Adams JD, Hu Z, Thundat T, Cavazos H, Minne SC (2003) Rev Sci Instrum 74:4899
46. Mertens J, Finot E, Nadal MH, Eyraud V, Heintz O, Bourillot E (2004) Sens Actuators B 99:58
47. Tang YJ, Fang J, Xu XH, Ji HF, Brown GM, Thundat T (2004) Anal Chem 76:2478
48. Yu XM, Zhang DC, Wang CS, Du XF, Wang XB, Ruan XB (2003) Chinese Phys Lett 20:1637
49. Abedinov N, Popov C, Yordanov Z, Ivanov T, Gotszalk T, Grabiec P, Kulisch W, Rangelow IW, Filenko D, Shirshov Y (2003) J Vac Sci Technol B 21:2931

50. Zhou J, Li P, Zhang S, Huang YP, Yang PY, Bao MH, Ruan G (2003) Microelectron Eng 69:37
51. Misna TE, McCorkle D, Warmack B (2003) Sens Actuators B 88:120
52. Fabre A, Finot E, Demoment J, Contreras S (2003) Ultramicroscopy 97:425
53. Fabre A, Finot E, Demoment M, Contreras S (2003) J Alloys Compd 356:376
54. Zhang YF, Ji HF, Brown GM, Thundat T (2003) Anal Chem 75:4773
55. Hilt JZ, Gupta AK, Bashir R, Peppas NA (2003) Biomed Microdevices 5:177
56. Liu K, Ji HF (200) Anal Sci 20:9
57. Zhang YF, Ji HF, Snow D, Sterling R, Brown GM (2004) Instrum Sci Technol 32:361
58. Zhou J, Li P, Zhang S, Long YC, Zhou F, Huang YP, Yang PY, Bao MH (2003) Sens Actuators B 94:337
59. Lee CY, Lee GB (2003) J Micromech Microeng 13:620
60. Muralidharan G, Wig A, Pinnaduwage LA, Hedden D, Thundat T, Lareau RT (2003) Ultramicroscopy 97:433
61. Pinnaduwage LA, Boiadjiev V, Hawk JE, Thundat T (2003) Appl Phys Lett 83:1471
62. Pinnaduwage LA, Thundat T, Gehl A, Wilson SD, Hedden DL, Lareau RT (2004) Ultramicroscopy 100:211
63. Pinnaduwage LA, Thundat T, Hawk JE, Hedden DL, Britt R, Houser EJ, Stepnowski S, McGill RA, Bubb D (2004) Sens Actuators B 99:223
64. Pinnaduwage LA, Wig A, Hedden DL, Gehl A, Yi D, Thundat T, Lareau RT (2004) J Appl Phys 95:5871
65. Pinnaduwage LA, Yi D, Tian F, Thundat T, Lareau RT (2004) Langmuir 20:2690
66. Weeks BL, Camarero J, Noy A, Miller AE, Stanker L, De Yoreo JJ (2003) Scanning 25:297
67. Yang YM, Ji HF, Thundat T (2003) J Am Chem Soc 125:1124
68. Gunter RL, Delinger WG, Manygoats K, Kooser A, Porter TL (2003) Sens Actuators A 107:219
69. Zhang J, Ji HF (2004) Anal Sci 20:585
70. Gfeller KY, Nugaeva N, Hegner M (2005) Biosens Bioelectron 21:528
71. Gfeller KY, Nugaeva N, Hegner M (2005) Appl Env Microbiol 71:2626
72. Alvarez M, Calle A, Tamayo J, Lechuga, LM, Abad A, Montoya A (2003) Biosens Bioelectron 18:649
73. Yan XD, Tang YJ, Ji HF, Lvov Y, Thundat T (2004) Instrum Sci Technol 32:175
74. Cherian S, Gupta RK, Mullin BC, Thundat T (2003) Biosens Bioelectron 19:411
75. Adams JD, Parrott G, Bauer C, Sant T, Manning L, Jones M, Rogers B, McCorkle D, Ferrell TL (2003) Appl Phys Lett 83:3428
76. Khaled ARA, Vafai K (2004) J Micromech Microeng 14:1220
77. Zhang Y, Ren Q, Zhao YP (2004) J Phys D 37:2140
78. Jeon S, Thundat T (2004) Appl Phys Lett 85:1083
79. Headrick JJ, Sepaniak MJ, Lavrik NV, Datskos PG (2003) Ultramicroscopy 97:417
80. Bottomley LA, Poggi MA, Shen SX (2004) Anal Chem 76:5685
81. Porter TL, Eastman MP, Macomber C, Delinger WG, Zhine R (2003) Ultramicroscopy 97:365
82. Kooser A, Gunter RL, Delinger WD, Porter TL, Eastman MP (2004) Sens Actuators B 99:474
83. Bumbu GG, Kircher G, Wolkenhauer M, Berger R, Gutmann JS (2004) Macromol Chem Phys 205:1713
84. Quist F, Tabard-Cossa V, Badia A (2003) J Phys Chem B 107:10691
85. Tian F, Pei JH, Hedden DL, Brown GM, Thundat T (2004) Ultramicroscopy 100:217
86. Su M, Li SU, Dravid, VP (2003) Appl Phys Lett 82:3562
87. Gunter RL, Zhine R, Delinger WG, Manygoats K, Kooser A, Porter TL (2004) IEEE Sensors J 4:430

88. Alvarez M, Carrascosa LG, Moreno M, Calle A, Zaballos A, Lechuga LM, Martinez-A C, Tamayo J (2004) Langmuir 20:9663
89. Gunter RL, Zhine R, Delinger WG, Manygoats K, Kooser A, Porter TL (2004) IEEE Sensors J 4:430
90. Lee JH, Yoon KH, Hwang KS, Park J, Ahn S, Kim TS (2004) Biosens Bioelectron 20:269
91. Lee JH, Kim TS, Yoon KH (2004) Appl Phys Lett 84:3187
92. Hwang KS, Lee JH, Park J, Yoon DS, Park JH, Kim TS (2004) Lab Chip 4:547
93. Kim BH, Mader O, Weimar U, Brock R, Kern DP (2003) J Vac Sci Technol B 21:1472
94. Kooser A, Manygoats K, Eastman MP, Porter TL (2003) Biosens Bioelectron 19:503
95. Saif MTA, Sager CR, Coyer S (2003) Annals Biomed Eng 31:950
96. Reasmussen PA, Thaysen J, Hansen O, Eriksen SC, Boisen A (2003) Ultramicroscopy 97:371
97. Arakawa ET, Lavrik NV, Rajic S, Datskos PG (2003) Ultramicroscopy 97:459
98. Yan XD, Lvov Y, Ji HF, Singh A, Thundat T (2003) Org Biomolec Chem 1:460
99. Liu F, Zhang Y, Ou-Yang ZC (2003) Biosens Bioelectron 18:655
100. Khaled ARA, Vafai K, Yang M, Zhang X, Orkan CS (2003) Sens Actuators B 94:103
101. Kumar S, Bajpai RP, Bharadwaj LM (2003) IETE Techn Rev 20:361
102. Zhang YF, Venkatachalan SP, Xu H, Xu XH, Joshi P, Ji HF, Schulte M (2004) Biosens Bioelectron 19:1473
103. Pei JH, Tian F, Thundat T (2004) Anal Chem 76:292
104. Yan XD, Ji HF, Lvov Y (2004) Chem Phys Lett 396:34
105. Ono T, Li XX, Miyashita H, Esashi M (2003) Rev Sci Instrum 74:1240
106. Ono T, Esashi M (2004) Meas Sci Technol 15:1977
107. Dufour I, Fadel L (2003) Sens Actuators B 91:353
108. Yum K, Wang ZY, Suryavanshi AP, Yu MF (2004) J Appl Phys 96:3933
109. Fadel L, Dufour I, Lochon F, Français O (2004) Sens Actuators B 102:73
110. Ryu WH, Chung YC, Choi DK, Yoon CS, Kim CK, Kim YH (2004) Sens Actuators B 97:98
111. Jeon S, Braiman Y, Thundat T (2004) Rev Sci Instrum 75:4841
112. Adams JD, York D, Whisman N (2004) Rev Sci Instrum 75:2903
113. Fadel L, Lochon F, Dufour I, Français O (2004) J Micromech Microeng 14:S23
114. Ren Q, Zhao YP (2004) In: Microsystem technologies, vol 10. Springer, Berlin Heidelberg New York, p 307
115. Kar AK, George MA (2003) J Appl Phys 94:4626
116. Sharos LB, Raman A, Crittenden S, Reifenberger R (2004) Appl Phys Lett 84:4638
117. Ilic B, Craighead HG, Krylov S, Senaratne W, Ober C, Neuzil P (2004) J Appl Phys 95:3694
118. Passian A, Muralidharan G, Mehta A, Simpson H, Ferell TL, Thundat T (2003) Ultramicroscopy 97:391
119. Tamayo J, Alvarez M, Lechuga LM (2003) Sens Actuators B 89:33
120. Tamayo J, Lechuga LM (2003) Appl Phys Lett 82:2919
121. Mertens J, Finot E, Thundat T, Falve A, Nadal MH, Eyraud V, Bourillot E (2003) Ultramicroscopy 97:119
122. Kim SJ, Hong KI, Choi DK (2003) J Appl Phys Pt 1 42:1475
123. Godin M, Laroche O, Tabard-Cossa V, Beaulieu LY, Grütter P, Williams PJ (2003) Rev Sci Instrum 74:4902
124. Gibson CT, Weeks BL, Abell C, Rayment T, Myhra S (2003) Ultramicroscopy 97:113
125. Hu ZY, Seeley T, Kossek S, Thundat T (2004) Rev Sci Instrum 75:400
126. Lin R, Boggild P, Hansen O (2004) J Appl Phys 96:2895
127. Khanafer K, Khaled ARA, Vafai K (2004) J Micromech Microeng 14:1328
128. Yue M, Lin H, Dedrick DE, Satyanarayana S, Majumdar A, Bedekar AS, Jenkins JW, Sundaram S (2004) J Microelectromech Syst 13:290